Non-invasive 4D Flow Characterization in a Stirred Tank via PC-MRI at 7T

Gábor Janiga[1], Daniel Stucht[2,3], Róbert Bordás[1], Erik Temmel[4], Andreas Seidel-Morgenstern[4], Dominique Thévenin[1], Oliver Speck[2,5]

1: Lab. of Fluid Dynamics and Technical Flows, University of Magdeburg "Otto von Guericke", Germany

2: Institute of Experimental Physics, University of Magdeburg "Otto von Guericke", Germany

3: Institute of Biometry and Medical Informatics, University of Magdeburg "Otto von Guericke", Germany

4: Max Planck Institute for Dynamics of Complex Technical Systems, Magdeburg, Germany

5: Leibniz Institute for Neurobiology, Magdeburg, Germany

Abstract The present work demonstrates that a non-invasive quantification of the hydrodynamics in a stirred tank in space and time is possible using flow sensitive phase-contrast magnetic resonance imaging (PC-MRI) at 7 Tesla (7T). The experimental technique has been developed for a batch crystallizer, but is applicable in principle for a variety of stirred-tank reactors and rotating systems. The PC-MRI technique is able to characterize the unsteady periodic three-dimensional flow velocities with acceptable spatial and temporal resolution, and does not imply that optically transparent fluids are employed. PC-MRI is already widely used for medical diagnostics in order to determine the blood flow velocities, e.g., for cardiovascular applications. However, the utilization of this method is still new for engineering problems, including process engineering. It is therefore important to check the applicability of PC-MRI to applications of practical interest in this field and complement other flow measurement and simulation techniques.

1 Introduction

Phase-contrast magnetic resonance imaging (PC-MRI) is a promising technique for the non-invasive characterization of hydrodynamics. This method is based on a gradient echo magnetic resonance imaging sequence that has been modified in order to encode the flow velocity in the phase of the measured signal . The higher signal-to-noise ratio (SNR) at 7-Tesla field strength enables a higher spatial resolution compared to systems with a lower magnetic field (typically 1.5 T or 3.0 T) and thus allows time-resolved three-dimensional MR-velocity mapping at higher resolution.

PC-MRI is already very widely used for medical diagnostics in order to characterize the hemodynamics for cardiovascular applications . Artificial models of human vascular anatomy-related geometries are also common . However, this measurement technique has been barely used for engineering problems, especially for chemical engineering applications . Such applications commonly involve opaque fluids or multiphase flows with a dense loading, for which optical techniques often cannot be applied. At the same time, characterizing hydrodynamic features is essential for most processes and it plays a key role during process design and optimization.

Considering crystallization, the application focused on specifically in the present work, the main parameters are impeller speed, impeller geometry, reactor geometry and the physical properties of the crystal suspension .

1

Unfortunately, the resulting hydrodynamics are usually very complex, impact directly the quality and quantity of crystal harvesting, and are difficult to predict numerically . The main task is to keep the crystals in suspension within a proper environment for growth without destroying them by collisions and attrition. Even if recent progress in coupled numerical approaches might lead to a better understanding of crystallization, it is absolutely necessary to validate these computational results with quantitative experimental data before proceeding further. The same applies to reaction engineering, for which a deeper insight in the underlying fluid dynamics would lead to improved process efficiency and safety by better control of heat and mass transfer . When dealing for instance with a highly exothermic reaction, the occurrence of a local hotspot due to a poorly mixed tank can lead to an uncontrolled reaction and therefore to unacceptable risks. For heterogeneous reactions the interstitial velocity between catalyst and educt mixture determines yield and efficiency of the process. The direct investigation of influencing parameters in systems with no or poor optical access would ultimately lead to enhanced performance and higher safety.

Among the measurement methods for velocity, particle-based techniques are widely used, with some well-known limitations. Firstly, obviously due to the nature of the methods, they rely on the presence of particles in the flow. Those should not only follow the smallest fluctuations of interest, but their number density must be also sufficient in order to reach the required spatial and temporal resolution, leading to difficult issues concerning seeding. Thus, particle motion in flows, scattering properties of tracer particles, particle or droplet generation and their proper introduction into the flow should be considered . At the same time, the seeding density should not exceed a certain level; otherwise, the resulting two-phase flow will be modified by the presence of the tracers. Fulfilling all these requirements simultaneously is in many cases very challenging. At the same time, the optical access to these tracers should be ensured as well. Assuming that the measurement fluid is transparent, which obviously already constitutes a major limitation, there are two main solutions in order to correct or avoid light distortion: 1.) Refractive index matching , using in many cases fluid mixtures with health and safety issues. Another issue that makes this method even more complicated is the sensitivity of the refractive index to temperature. 2.) The other possibility is to perform an optical correction by computational post-processing . This second method also has its limitations, since if the critical angle is reached during light refraction retrospective corrections become impossible.

Alternative techniques that allow hydrodynamic measurements in opaque reactors, such as tomography or tracking radioactive particles (CARPT) are quite complex and have already been discussed in review articles . Especially CARPT is widely applicable also in ferromagnetic environments in contrary to PC-MRI. In this technique, single gamma-emitting particles of a radioactive component are utilized that are followed by arrays of precise scintillation detectors . The particles are prepared and polymer-coated to match the density of the liquid or solid phase that is investigated with respect to the fluid dynamics in a certain setup. Thus, the radioactive material follows the same streamlines as the phase of interest and hence velocities and pathways can be estimated applying, e.g., Monte-Carlo methods together with the experimental results. This technique was already successfully applied to industrial processes, fluidized bed and stirred-tank setups . However, the preparation of a radionuclide material starting from the synthesis followed by e.g., calcination, coating and activation in a corresponding reactor is challenging and has to be conducted in special laboratories . Subsequently, the produced phase must be characterized precisely with respect to density, surface properties, emitted gamma spectrum and intensity. Together with the extensive effort for calibration of the detectors, the

sophisticated CARPT method seems to be too complex for common industrial problems even though accurate data of the fluid dynamics can be acquired.

Due to the increasingly successful application of PC-MRI in the medical field, its application to engineering flows has increasingly been considered in the last years. For example, the mean velocity values in complex turbulent flows have been measured in , while the measurement of turbulent quantities are discussed in . For a comprehensive overview of the application of PC-MRI for non-medical applications, we refer to excellent review articles and to the references therein.

Additionally to the determination of two- or three-dimensional velocities for steady or transient flows, the measurement of other quantities is also of great importance in various process engineering applications. The experimental investigation of the three-dimensional concentration field in a mixing layer using MRI has been reported in and the simultaneous determination of the velocity and scalar field for an airfoil trailing edge is discussed in . MRI for microfluidic devices has been also considered . The mixing behavior was the subject of the study published by .

The measurement of multi-component or multi-phase flows is particularly interesting in order to improve and further optimize existing industrial configurations. Bieberle et al. have investigated two-phase flows with MRI. The gas dynamics in a cavitating liquid including void fraction have been characterized in . Neacsu et al. have studied the impregnation induced by capillarity across aligned cylinders. Granular flows measured using MRI are discussed in several studies . Wheat grain cooking process was the subject of the work by .

Despite a growing number of PC-MRI applications for engineering configurations, no reports could be found in the literature yet concerning rotating systems. Such applications are of course very challenging, since a non-ferromagnetic system has to be developed before characterization by PC-MRI, including all control lines and periphery. The current work attempts to close this gap by applying PC-MRI in a stirred batch reactor. In such systems, the hydrodynamics is particularly important for an appropriate mixing and therefore for reaching the targeted product quality. In this first investigation the complex three-dimensional unsteady flow in a stirred tank representing a rotating batch crystallizer is considered. The obtained results will be used to support the validation of companion simulations relying on computational fluid dynamics (CFD).

This proof of concept study aims at giving more insight into the complex flow in a stirred tank. The paper is organized as follows. First, the investigated stirred tank geometry is described. Then, the measurement method is presented. The experimental results are then used to quantify the hydrodynamic properties in the reactor. Finally, the key findings are summarized.

2 Phase Contrast MRI principles

The basic principle of most MRI sequences is that the hydrogen nucleus processes around the external magnetic field with the Larmor frequency ω. The precession frequency rises linearly with the field strength. At 7T the Larmor frequency of a hydrogen nucleus is about 298 MHz. The resulting MR signal is complex-valued. As the Larmor frequency depends on the magnetic field strength, it is possible to encode, e.g., spatial information by locally changing the magnetic field strength using magnetic field gradients. Readers who would like to know more about basic MR acquisition principles can find more detailed information in reference

publications . By applying a gradient, the frequency of the nuclei is changed, causing a position-dependent phase difference. When a reversed gradient is applied, this phase difference is cancelled for all stationary protons. Only if a proton experienced a change in position along the gradient direction during this bipolar gradient, a phase difference will result. These phase differences contain the flow information. Other effects can also cause phase changes of the signal, which have to be corrected for by acquiring a reference scan without flow encoding, only containing the so-called background phase, which is then subtracted from the flow-sensitive scans. The maximum velocity encoded in a full signal phase rotation is determined by the strength and duration of the bipolar flow encoding gradients and specified by the velocity encoding parameter (v_{enc}). To avoid phase wraps, this parameter should be set above the highest velocity to be expected, but not much higher, as the measure of slow velocities for higher v_{enc} parameters shows a lower velocity-to-noise ratio (VNR). As the flow-encoding gradients can only be applied in one direction at a time, at least three acquisitions (one for each velocity vector-component u, v and w) and one reference scan are necessary. In MRI, an image is usually not obtained in real time. Instead a raw data matrix of the frequency domain, the so-called k-space, is acquired line by line with different encoding schemes to form a full k-space. K-space can be converted to image space by applying an inverse Fourier transformation creating the final MR-image. For medical applications, the magnitude image represents the anatomical features, while the phase image is often discarded. In PC-MRI, the flow information is instead encoded in the phase images. Because of the line-by-line k-space acquisition, dynamic flow processes measured with phase contrast MRI must be of a repetitive nature. This is a major, intrinsic limitation of the process, since the acquisition frequency is relatively low with standard imaging methods, due to the high number of encoding steps as outlined above. To represent the dynamic nature of such processes, multiple images of different time points of one cycle are acquired over time to produce a time-resolved dataset (CINE-MRI). During each cycle, only a small number of k-space lines can be acquired per time point, so that the complete acquisition requires measurements over many cycles. Therefore, the signal acquisition is synchronized to an appropriate trigger, allowing to sort a posteriori the acquired k-space lines to multiple images for several time points in the repeating cycle.

In the present case, a stirred reactor is considered that is driven at a constant rotation frequency. Due to the periodic nature of the flow and an appropriate trigger signal it is possible to reconstruct the dynamic but periodic data from individual measurements acquired over many rotations.

3 Experimental setup

Investigations of a stirred tank reactor inside an MR scanner with a field strength of 7 Tesla is an unusual application that leads to several requirements for the experimental setup. Obviously no ferromagnetic material can be used inside the PC-MRI laboratory room. Due to susceptibility effects, other metals such as aluminum also have to be excluded from the measurement volume. Only limited space is available within the radio-frequency transmit and receive coil so that small-size components must be machined. Furthermore, any compressor and pump used for driving the impeller had to be placed outside the scanner room, behind a radio frequency shielding, approximately 15 meters away from the MRI system. To overcome these obstacles a dedicated stirred tank was constructed (Fig. 1).
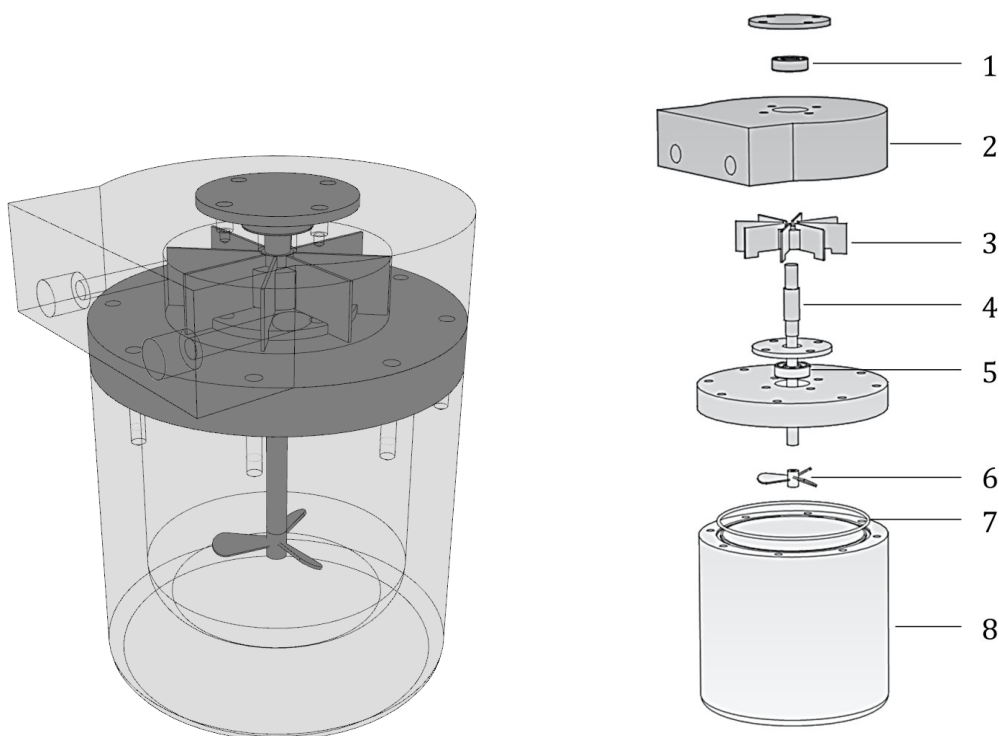
Fig. 1 CAD model and exploded drawing of the reactor utilized for the PC-MRI experiments. Parts: PTFE ball bearings (1, 5); cover (2); fan wheel (3); stirrer shaft (4); turbine impeller (6); sealing (7); reactor body (8).

Most of the reactor was manufactured from polycarbonate. Thus, no interaction of the material with the magnetic field is expected. The overall height of the complete unit is 160 mm with a diameter of 120 mm and a maximum mixing volume of 550 ml. Compressed air was chosen to drive the stirrer instead of water, in order to reduce the risk of damaging the MRI unit if a leak should occur. Therefore, a fan wheel (3 in Fig. 1) was installed at the top of the stirrer shaft (4 in Fig. 1) as a power coupling. The shaft is supported by two polymer ball bearings (1, 5 in Fig. 1, Company: Buehring-Adam Germany, special model type 608). Finally, a turbine impeller (6 in Fig. 1) was used to constantly mix the liquid content of the reactor (8 in Fig. 1) during the experiment. All parts in Fig. 1 beside the ball bearings were designed and manufactured at the Max Planck Institute for Dynamics of Complex Technical Systems in Magdeburg. In order to produce as few artifacts as possible and to ensure consistent time resolved acquisition, the stirrer speed had to be constant during the measurements. This was implemented by a mass flow controller (Range: 0-100 rpm, Company: Bronkhorst Germany) connected to a potentiometer and used to adjust the airflow. The model substance employed for the following experiments was water with 0.9 wt-% of NaCl. NaCl was added in order to change the electric conductivity. The propagation parameter of the electric field depends on the material. By adding NaCl, the dielectric constant is changed, standing wave effects are reduced and the signal homogeneity of the images is increased. Of course, it is not necessary to use such a transparent fluid for the considered experiments. Using water was just straightforward and convenient.

In order to synchronize the PC-MRI system with the periodic flow inside the stirrer reactor, a triggering scheme had to be realized. The generation of TTL signals was associated with the position of the fan wheel (part Nr. 3 in Fig. 1) and thus indirectly with the angular position of the turbine impeller (6 in Fig. 1). The

identification of the zero position of the fan wheel was obtained by using a photo-electric sensor and an LED. The latter produced a nearly monochromatic light, bundled into an optical fiber. Since optical fibers are nonmagnetic, the light could be led directly to the stirrer reactor placed inside the PC-MRI. One blade of the fan wheel was marked with a luminous paint, reflecting back the light into another optical fiber to the electric circuit in the control room (Fig. 2). Here, the light signals were transformed into electric signals by means of a photo diode. Finally, a microprocessor generated TTL signals from these electric signals, used finally to synchronize the angular position of the impeller with the phases of the PC-MRI acquisition.

The final measurement has been realized with a constant rotation speed of 98.8 rpm, corresponding to 1.65 revolutions per seconds. A single revolution is measured at 22 time instants yielding a time difference of 28 ms between two consecutive measurements.


4 Measurement method

4D Phase-contrast MRI measurements have been performed using a 7-Tesla MRI system (Siemens Medical Solutions, Germany) and a 32-channel head coil (Nova Medical, Wilmington, MA, USA). The reactor was placed in the coil and kept in place with restraints such as cushions and pads in order to avoid any motion during the measurement. A water-level was used to ensure a proper horizontal orientation. The compressor and the trigger device had to be placed outside the scanner room to avoid any radio frequency interference. Hence, all pipes and optical fibers had to be led through a wave guide.

The flow data were acquired using 4D PC-MRI , which is based on a triggered and radio frequency-spoiled gradient echo (GRE) sequence. The scan parameters were: repetition time/echo time 7.0 ms/4.115 ms, temporal resolution: 28 ms, 21 temporal phases, flip angle: 5 deg., bandwidth: 450 Hz/pixel, parallel imaging (GRAPPA) factor 2, total acquisition time: approx. 54 min., v_{enc} 0.3 m/s, matrix 128x128x72 pixel, FOV 160x160x90 mm, 1.25 mm isometric voxelsize. Given the known diameter of the reactor and impeller blades, the maximum velocities were estimated accordingly. No phase-wraps were observed in the measured data. To correct for eddy current artifacts, the same measurements but without activated flow inside the reactor were acquired for reference. These scans were subtracted from the flow scans to obtain purely flow related phase differences. To increase the temporal resolution, all scans were repeated with a trigger delay of one half phase, i.e. a shift of 14 ms.

The data were post processed using MeVisLab 2.3.1 (MeVis Medical Solutions AG, Bremen, Germany, www.mevislab.de). The background phase effects are of rather low spatial frequency, thus the reference data without flow were median filtered to reduce noise. Afterwards, the median filtered background phase was subtracted from the actual flow data. In addition, the background noise in areas without signal was removed by masking. The mask was derived by summing over all time-steps of the magnitude data and a threshold level was applied on this sum. Further steps of the post-processing were carried out using the automated tool described in . This included noise masking, antialiasing and conversion to the format of the commercial software package EnSight (CEI, Apex, NC, USA)

As described above, an optical sensor, delivering a signal after every full cycle was used for triggering the sequence. With the specified temporal resolution, a full rotation would consist of 22 full phases. If the next trigger signal is send before all expected time steps were scanned, the data scanned during the last revolution is

rejected and rescanned. If that happens often, the scan time increases dramatically. As a precaution for small fluctuations in the rotation frequency only 21 phases were measured.
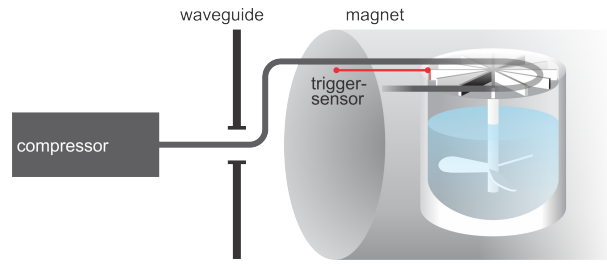
Fig. 2 Schematic illustration of the experimental setup.

5 Experimental results

The measured velocity magnitude is shown in Fig. 3 in two selected cut-planes for a selected impeller position. The impeller rotated in the clockwise direction (viewed from the top) pushing the fluid down. The highest velocities in the laboratory frame are shown by red colors. They are located close to the tip of the impeller blades.

The velocity vectors corresponding to these same cut-planes as in Fig. 3 are shown in Fig. 4. As the impeller rotated in the clockwise direction as viewed from above, the fluid is pushed down as shown by the longer red vectors. Far from the impeller blades the velocity vectors are directed upwards in the same horizontal plane. (The complete series of all the measured time-steps are available as a video on the homepage of the journal as Supplementary Information [*MRI_Animation_Velocities__Janiga_et_al.mpg*]).

Pathlines computed from the measured velocity field – sometimes called also particle traces assuming massless particles following perfectly the fluid flow – can be computed from all the available time-steps and assuming a perfectly periodic flow (Fig. 5). Pathlines can be emitted from various locations as well as starting from different time instants. They are particularly useful to reveal the complex structure of a transient fluid flow. The computation of streamlines is conceptually much easier than pathlines, because they are integrated for a frozen time-step. However, animating streamlines in rotating configurations is awkward, because these lines might cross the rotating solid parts (impeller blades). This is why pathlines are to be preferred when available. Pathlines emitted from the horizontal plane at the height of the impeller are shown in Fig. 5 integrated for a single rotation cycle. As it is portrayed in Fig. 5 the impeller pushes the fluid downward, but close to the wall of the tank, the pathlines are directed upward.

Time-averaged velocities are depicted in Fig. 6 for a single revolution in the laboratory frame. These averaged values show a smooth distribution of the velocity field reducing the measurement uncertainty. However, due to the time-averaging dynamic flow effects are not capured in this representation. Fig. 6 (left) depicts the movement of the velocity close to the blades, while the in-plane streamlines (Fig. 6 (right)) illustrate the global recirculation in the tank.

The measured flow velocities can also be investigated in the rotating reference frame of the impeller

instead of the laboratory frame. The time-averaged velocities are represented in Fig. 7 for a horizontal plane close the impeller blades. Fig. 7 (left) shows the velocities in the laboratory (absolute) frame revealing the maximum values close to the tip of the blades. Fig. 7 (right) depicts the velocity vectors in the rotating frame. As expected the largest velocities appear at the wall of the tank in this rotating frame, while the smallest values are close the blades. The temporal variation of the velocities is negligible, proving that the flow can be considered as steady in the rotating reference frame. The time averaging reduced the measurement noise even further allowing a smoother representation.
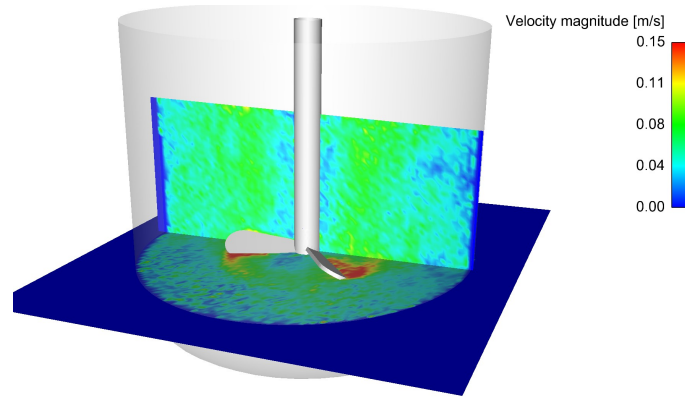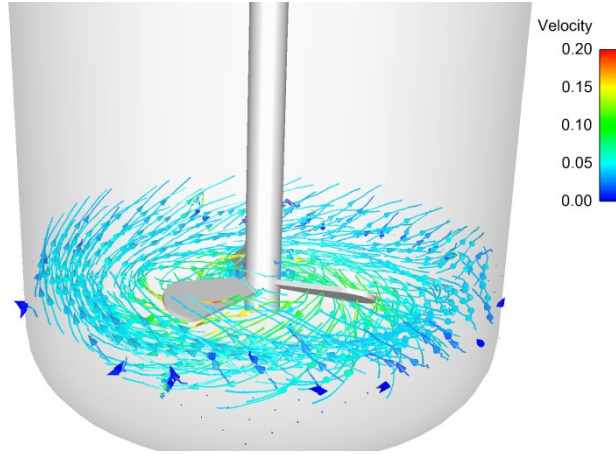

**Fig. 3** Measured phase-averaged velocity magnitude in two selected cut-planes for a specific impeller position.
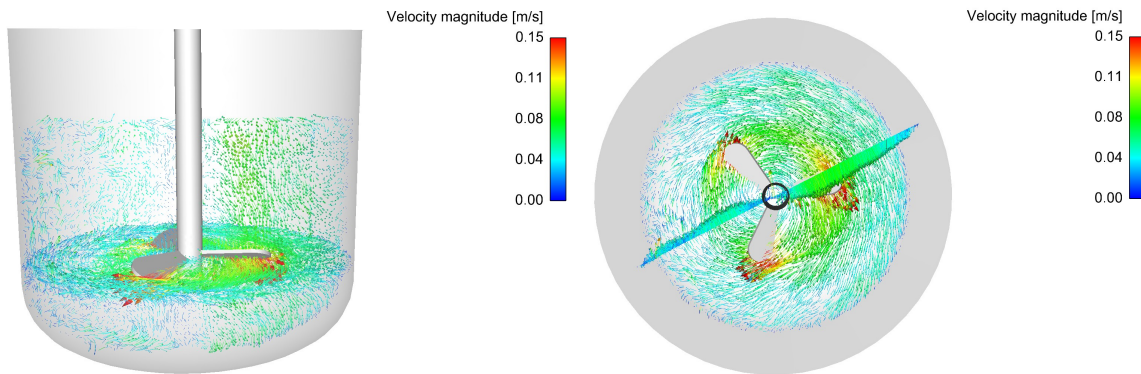
Fig. 4 Measured phase-averaged velocity vectors in two selected cut-planes for a specific impeller position (same cut-planes as in Fig. 3).

8

Fig. 5 Pathlines of the measured velocity, emitted in the horizontal plane of the impeller, colored by velocity magnitude. The pathlines are integrated during a complete revolution of the impeller (same views as in Fig. 4). The represented impeller position corresponds to its final position after the revolution.
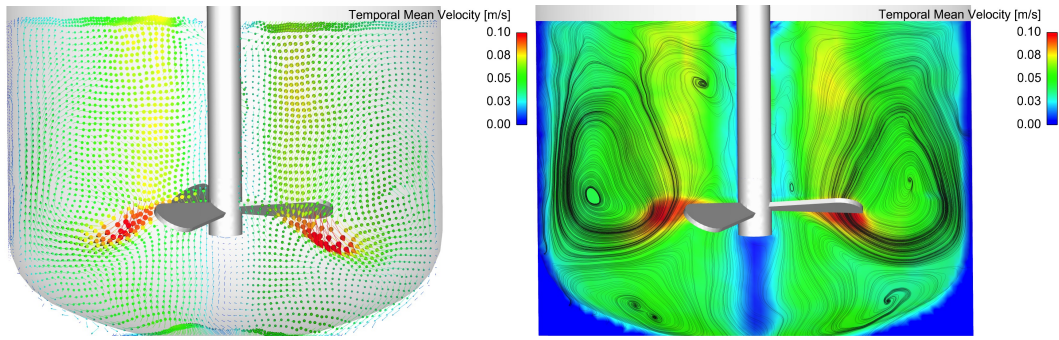
Fig. 6 Time-averaged velocities computed for a single revolution. Left: velocity vectors in a vertical middle plane. Right: in-plane streamlines of the temporal averaged velocities in the same vertical plane, and contours of velocity magnitude.
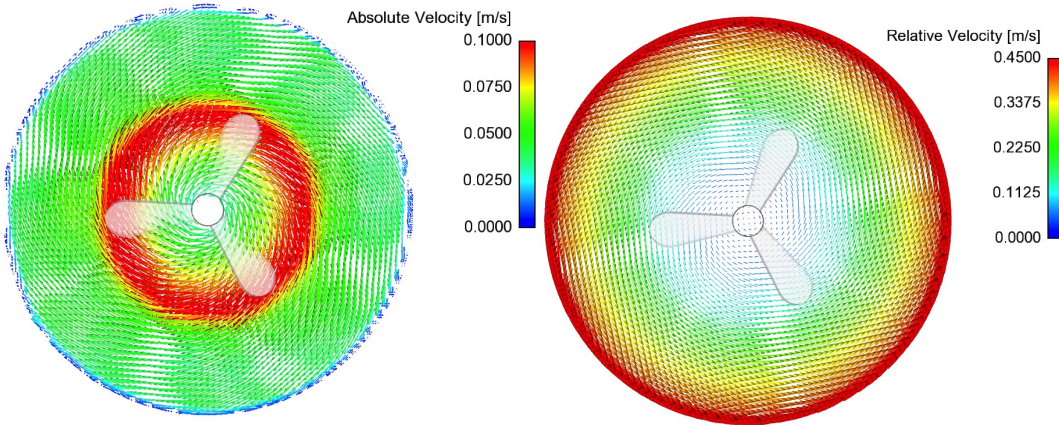
Fig. 7 Time-averaged velocities computed for a single revolution. Left: velocity vectors in a horizontal plane close to the impeller blades in the laboratory frame. Right: velocity vectors in the rotating frame in the same horizontal plane. The rotation of the impeller is in the clockwise direction in the presented top views.

9

6 Limitations

The common limitations for MRI scans also apply for this measurement. The object being scanned needs to be free of metal, because any metal would cause strong artifacts and signal dropouts. If the material is ferromagnetic, the strong magnetic forces would attract the object which might be dangerous and lead to harmful accidents. Beside these typical limitations for MRI, not all flow behavior can be imaged with this method. The flow needs to be of a stationary or at least repetitive nature, e.g., pulsatile or rotational. This is due to the fact, that the data cannot be acquired in one single measurement, such as in photography, but merely require many measurements to fill the so called k-space line by line, before it is transformed to image space via an FFT. For that reason, the scan is synchronized to the periodicity of the impellers rotation, if temporal resolution is required. This way, every single measurement (every measured k-space line) can be related to a certain temporal phase and thus for every temporal phase, a complete dataset is successively acquired. The number of temporal phases is limited by the time needed to measure one k-space line, usually called the repetition time (TR). In the case of 4D Flow measurement, four lines need to be scanned to measure the flow information in all the three Cartesian directions including one reference line. Thus, the temporal resolution is limited to four times the repetition time.

7 Conclusion

This paper has documented the successful application of PC-MRI for the determination of unsteady periodic three-dimensional flow velocities for a process engineering application. The complete flow field has been characterized in a stirred batch crystallizer in a non-invasive way.

It has been shown that detailed information can be obtained concerning hydrodynamics. However, the realization of the experiment in a stirred tank was particularly challenging since no ferromagnetic part could be used. Despite these difficulties, all associated issues could be successfully solved, as documented in this article.

Since a complete velocity characterization in space and time is available after a careful data processing, various flow visualization techniques can be afterwards applied. As an example, detailed information on the transient three-dimensional velocity – both in terms of magnitude as well as vectors – has been presented, together with flow pathlines.

8 Outlook

Adjusting the triggering scheme of the MRI sequence instead of repeating it with a trigger delay would allow an even higher temporal resolution and the coverage of a full cycle. After changing the sequence and post-processing pipeline accordingly, a reference database for stirred tanks without optical access will be developed.

For many applications, it is very challenging to create models without any metallic parts. New manufacturing methods such as rapid prototyping will simplify the process of creating complex MR-compatible models.

References

[1]   M. Markl, F. P. Chan, M. T. Alley, K. L. Wedding, M. T. Draney, C. J. Elkins, D. W. Parker, R. Wicker, C. A. Taylor, R. J. Herfkens, *J Magn Reson Imaging*, **2003***, 17 (4),* 499-506.
[2]   M. Markl, A. Harloff, T. A. Bley, M. Zaitsev, B. Jung, E. Weigang, M. Langer, J. Hennig, A. Frydrychowicz, *J Magn Reson Imaging*, **2007***, 25 (4),* 824-831.
[3]   P. Berg, D. Stucht, G. Janiga, O. Beuing, O. Speck, D. Thévenin, *J Biomech Eng*, **2013***, 136,* 041003/1-9. DOI: 10.1115/1.4026108
[4]   M. Markl, A. Frydrychowicz, S. Kozerke, M. Hope, O. Wieben, *J Magn Reson Imaging*, **2012***, 36 (5),* 1015-1036. DOI: 10.1002/jmri.23632
[5]   K. W. Moser, E. C. Kutter, J. G. Georgiadis, R. O. Buckius, H. D. Morris, J. R. Torczynski, *Exp Fluids*, **2000***, 29,* 438-447.
[6]   E. H. Hardy, *Chem. Eng. Technol.*, Review, **2006***, 29 (7),* 785-795. DOI: 10.1002/ceat.200600046
[7]   J. W. Mullin, *Crystallization*, Butterworth-Heinemann, Oxford **1993**.
[8]   B. Ashraf Ali, G. Janiga, E. Temmel, A. Seidel-Morgenstern, D. Thévenin, *J Cryst Growth*, **2013***, 372,* 219–229. DOI: 10.1016/j.jcrysgro.2013.01.041
[9]   M. Bearns, A. Behr, A. Brehm, J. Gmehling, H. Hofmann, U. Onken, A. Renken, *Technische Chemie*, Wiley-VCH, Weinheim **2006**.
[10]   E. L. Cussler, *Diffusion: Mass transfer in fluid systems*, Cambridge University Press, Cambridge **2009**.
[11]   C. Tropea, L. Yarin, J. F. Foss, *Handbook of experimental fluid mechanics*, Springer, Berlin **2007**.
[12]   N. Amini, Y. A. Hassan, *Exp Fluids*, **2012***, 53 (6),* 2011-2020.
[13]   R. Budwig, *Exp Fluids*, **1994***, 17 (5),* 350-355.
[14]   R. Bordás, S. Seshadhri, G. Janiga, M. Skalej, D. Thévenin, *Interv Med Appl Sci*, **2012***, 4 (4),* 193-205 DOI: 10.1556/IMAS.4.2012.4.4
[15]   A. S. Glassner, *An introduction to ray tracing*, Morgan Kaufmann Publishers, Inc., San Francisco, CA **1989**.
[16]   F. Scarano, L. David, M. Bsibsi, D. Calluaud, *Exp Fluids*, **2005***, 39 (2),* 257-266. DOI: 10.1007/s00348-005-1000-x
[17]   M. P. Dudukovic, *Exp Thermal Fluid Sci*, **2002***, 26,* 747-761.
[18]   P. Mavros, *Trans IChemE*, **2001***, 79(A),* 113-127.
[19]   J. Biswal, S. Goswami, H. J. Pant, Y. R. Bamankar, T. V. R. V. Rao, R. K. Upadhay, A. Dash, *Ind. Eng. Chem. Res.*, **2015***, 55 (1),* 3-12.
[20]   N. Ali, T. Al-Juwaya, M. Al-Dahhan, *Exp Thermal Fluid Sci*, **2017***, 80,* 90–104.
[21]   W. S. Vieira, L. E. B. Brandão, D. Braz, *Appl. Radiat. Isot.*, **2014***, 85,* 139–146.
[22]   C. Elkins, M. Markl, N. Pelc, J. Eaton, *Exp Fluids*, **2003***, 34 (4),* 494-503.
[23]   C. J. Elkins, M. T. Alley, L. Saetran, J. K. Eaton, *Exp Fluids*, **2009***, 46 (2),* 285-296. DOI: 10.1007/s00348-008-0559-4
[24]   C. J. Elkins, M. T. Alley, *Exp Fluids*, **2007***, 43 (6),* 823-858.
[25]   L. F. Gladden, A. J. Sederman, *J Magn Reson*, **2013***, 229,* 2-11.
[26]   M. J. Benson, C. J. Elkins, P. D. Mobley, M. T. Alley, J. K. Eaton, *Exp Fluids*, **2010***, 49 (1),* 43-55.
[27]   M. J. Benson, C. J. Elkins, J. K. Eaton, *Exp Fluids*, **2011***, 51,* 443-455. DOI: 10.1007/s00348-011-1062-x
[28]   T. Z. Teisseyre, J. L. Paulsen, V. S. Bajaj, N. W. Halpern-Manners, A. Pines, *J Magn Reson*, **2012***, 216,* 13-20. DOI: 10.1016/j.jmr.2011.10.001
[29]   E. J. Tozzi, K. L. McCarthy, L. A. Bacca, W. H. Hartt, M. J. McCarthy, *J Visualized Exp*, **2012***, 59,* e3493/1-e3493/9.
[30]   M. Bieberle, F. Fischer, E. Schleicher, D. Koch, H. J. Menz, H. G. Mayer, U. Hampel, *Exp Fluids*, **2009***, 47,* 369-378. DOI: 10.1007/s00348-009-0617-6

[31]   I. V. Mastikhin, A. Arbabi, B. Newling, A. Hamza, A. Adair, *Exp Fluids*, **2012***, 52,* 95-104. DOI: 10.1007/s00348-011-1209-9

[32]   V. Neacsu, J. Leisen, H. W. Beckham, S. G. Advani, *Exp Fluids*, **2007***, 42,* 425-440. DOI: 10.1007/s00348-007-0251-0

[33]   M. Nakagawa, S. A. Altobelli, A. Caprihan, E. Fukushima, E. K. Jeong, *Exp Fluids*, **1993***, 16,* 54-60.

[34]   P. Porion, N. Sommier, P. Evesque, *Europhys Lett*, **2000***, 50 (3),* 319-325.

[35]   P. Porion, N. Sommier, A.-M. Faugère, P. Evesque, *Powder Technol*, **2004***, 141,* 55-68.

[36]   A. G. F. Stapley, T. M. Hyde, L. F. Gladden, P. J. Fryer, *Int J Food Sci Tech*, **1997***, 32 (5),* 355-375.

[37]   M. A. Brown, R. C. Semelka, *MRI: Basic principles and applications*, 4th ed., John Wiley & Sons, Inc., Hoboken, NJ **2010**.

[38]   E. M. Haacke, R. W. Brown, M. R. Thompson, R. Venkatesan, *Magnetic resonance imaging: Physical principles and sequence design*, John Wiley & Sons, Inc., New York **1999**.

[39]   J. Bock, B. Kreher, J. Hennig, M. Markl, *Proc. Intl. Soc. Mag. Reson. Med.*, **2007***,* 3135.